Numerical methods based on regularized δ-distributions

1 Blobs in one dimension

Let $\phi(x) : \mathbb{R} \to \mathbb{R}$ be a smooth even function satisfying $\int_{-\infty}^{\infty} \phi(x)dx = 1$. Examples of these functions are

$$\phi(x) = \frac{1}{\sqrt{\pi}}\, e^{-x^2} \qquad \textit{and} \qquad \phi(x) = \frac{1}{2(x^2+1)^{3/2}}.$$

A blob ϕ_δ in one dimension is defined as a scaled version of one of these functions,

$$\phi_\delta(x) = \frac{1}{\delta}\phi(x/\delta)$$

where the scaling parameter δ is small. Notice that for any value $\delta > 0$, the blob satisfies

$$\int_{-\infty}^{\infty} \phi_\delta(x)dx = \int_{-\infty}^{\infty} \frac{1}{\delta}\phi(x/\delta)dx = \int_{-\infty}^{\infty} \phi(z)dz = 1 \quad (\text{let } z = x/\delta)$$

while at the same time $\phi_\delta(0) = \phi(0)/\delta$. This indicates that for small values of δ, the value of $\phi_\delta(0)$ is large but the blob is very narrow, and for large values of δ, the blob is smaller but wider (see Figure 1).

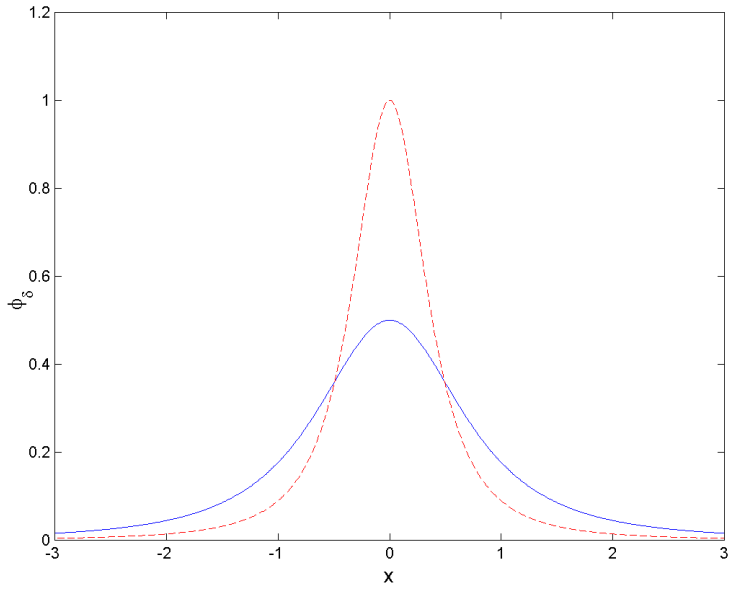

Figure 1: Sample blob for two different values of δ.

Consider a smooth function $f(x)$ and the convolution function

$$(f \star \phi_\delta)(x) = \int_{-\infty}^{\infty} f(y)\phi_\delta(x-y)\ dy.$$

One can imagine that if δ is very small, the blob is concentrated near $y = x$, and so the integral will have contributions mostly from values of y near x, and therefore the convolution should not be too different from $f(x)$.

More precisely, let $f(x)$ have n continuous derivatives. Since

$$(f \star \phi_\delta)(x) = \int_{-\infty}^{\infty} f(y)\phi_\delta(x-y)\ dy$$

we can let $\delta z = x - y$ and and use the fact that $\phi_\delta(x-y) = \frac{1}{\delta}\phi(z)$ we have that

$$(f \star \phi_\delta)(x) = \delta \int_{-\infty}^{\infty} f(x-\delta z)\phi_\delta(\delta z)\ dz = \int_{-\infty}^{\infty} f(x-\delta z)\phi(z)\ dz.$$

Now, Taylor's theorem with remainder gives

$$f(x-\delta z) = f(x) + \sum_{k=1}^{n-1} \frac{1}{k!}(-\delta)^k z^k f^{(k)}(x) + \frac{1}{n!}(-\delta)^n z^n f^{(n)}(\xi).$$

Then the convolution is

$$\begin{aligned}(f \star \phi_\delta)(x) \ &= \ f(x)\int_{-\infty}^{\infty}\phi(z)\ dz + \sum_{k=1}^{n-1}\frac{1}{k!}(-\delta)^k f^{(k)}(x)\int_{-\infty}^{\infty} z^k\phi(z)\ dz \\ &\quad + \frac{1}{n!}(-\delta)^n \int_{-\infty}^{\infty} f^{(n)}(\xi) z^n \phi(z)\ dz\end{aligned}$$

Let $M_k(\phi) = \int_{-\infty}^{\infty} z^k\phi(z)\ dz$ (known as the k-th *moment* of the function ϕ), then

$$(f \star \phi_\delta)(x) = f(x)M_0(\phi) + \sum_{k=1}^{n-1}\frac{1}{k!}(-\delta)^k f^{(k)}(x)M_k(\phi) + O(\delta^n)$$

or

$$(f\star\phi_\delta)(x) = f(x)M_0(\phi) - \delta f'(x)M_1(\phi) + \frac{1}{2!}\delta^2 f''(x)M_2(\phi) - \frac{1}{3!}\delta^3 f'''(x)M_3(\phi) + \cdots + O(\delta^n).$$

This formula tells us how to make the difference between $(f \star \phi_\delta)(x)$ and $f(x)$ small.

- If we make a blob ϕ such that $M_0(\phi) = 1$, then $(f \star \phi_\delta) - f = O(\delta)$.

- If we make a blob ϕ such that $M_0(\phi) = 1$ and $M_1(\phi) = 0$, then $(f \star \phi_\delta) - f = O(\delta^2)$.
- If we make a blob ϕ such that $M_0(\phi) = 1$ and $M_k(\phi) = 0$ for $k = 1, ..., p-1$, then $(f \star \phi_\delta) - f = O(\delta^p)$.

1.1 Numerical approximation of convolutions

Assume that $f(x)$ is zero outside the interval $[a, b]$. In a numerical method, whenever we use the convolution $(f \star \phi_\delta)(x)$ to approximate $f(x)$, we must approximate the integral

$$(f \star \phi_\delta)(x) = \int_a^b f(y)\phi_\delta(x - y)\, dy.$$

To do this, let's suppose we know the values of the function f at N points on the interval $[a, b]$. So we have the data (y_k, f_k) for $k = 1, 2, \cdots, N$ and we require that $y_1 = a$ and $y_N = b$. In this case, the spacing between points does not have to be uniform.

Now the integral can be approximated with the trapezoid rule

$$\begin{aligned}(f \star \phi_\delta)(x) &\approx \frac{(y_2 - y_1)}{2} f_1 \phi_\delta(x - y_1) + \frac{(y_N - y_{N-1})}{2} f_N \phi_\delta(x - y_N) \\ &+ \sum_{k=2}^{N-1} \frac{(y_{k+1} - y_{k-1})}{2} f_k \phi_\delta(x - y_k) \\ &= \sum_{k=1}^{N} h_k f_k \phi_\delta(x - y_k) \qquad (1)\end{aligned}$$

where, as before, $h_1 = (y_2 - y_1)/2$, $h_N = (y_N - y_{N-1})/2$, and $h_k = (y_{k+1} - y_{k-1})/2$ for all others.

Example 1.1 Consider the two blobs:

$$\phi_1(x) = \frac{1}{\sqrt{\pi}}\, e^{-x^2}, \qquad \phi_2(x) = \frac{1}{2\sqrt{\pi}}(3 - 2x^2)\, e^{-x^2},$$

which satisfy $M_0 = 1$ and $M_1 = 0$ but $M_2(\phi_1) = 1/2$ and $M_2(\phi_2) = 0$, $M_4(\phi_2) = -3/4$. Suppose we want to use these to approximate the function $f(x) = [1 + \cos(2\pi x)]^2$ for $-1/2 \le x \le 1/2$ and we use $\delta = 0.01$. The results are

$$\|(f \star \phi_{\delta 1}) - f\|_\infty = 3.943 \times 10^{-3} \quad \textit{and} \quad \|(f \star \phi_{\delta 2}) - f\|_\infty = 4.860 \times 10^{-6}$$

which shows how much better the results are with the blob derived from ϕ_2.

Based on our results, the error in ϕ_1 is estimated by $max|f''(x)M_2(\phi_1)/2| \approx 80(1/2)\delta^2 = 4 \times 10^{-3}$. For ϕ_2, the error is estimated by $max|f^{(4)}(x)M_4(\phi_2)/24| \approx 650(3/4)\delta^4 = 4.875 \times 10^{-6}$. We can see that the errors in our numerical solution are consistent with the estimates.

Example 1.2 Suppose $N = 21$, $[a, b] = [-1, 1]$ and $h = (b-a)/(N-1) = 0.1$, and that the data (y_k, f_k) are given in the table below.

y_k	f_k	y_k	f_k
-1.0000	0.0000	0.0000	0.7071
-0.9000	0.0785	0.1000	0.7604
-0.8000	0.1564	0.2000	0.8090
-0.7000	0.2334	0.3000	0.8526
-0.6000	0.3090	0.4000	0.8910
-0.5000	0.3827	0.5000	0.9239
-0.4000	0.4540	0.6000	0.9511
-0.3000	0.5225	0.7000	0.9724
-0.2000	0.5878	0.8000	0.9877
-0.1000	0.6494	0.9000	0.9969
		1.0000	1.0000

Then the function $f(x)$ that the data represent is approximated by the function $g(x) = \sum_{k=1}^{N} h_k f_k \phi_\delta(x - y_k)$, with the spacing h_k given as in the previous discussion. Any choice of blob ϕ_δ will give a slightly different approximation, however, the errors should be comparable when using blobs that satisfy the same moment conditions. Once we choose a blob, we must choose the value of the parameter δ. This must be of similar size as the particle spacing h_k (or the maximum spacing).

In this example, since $h_k = h = 0.1$ for all k, we might decide to set $\delta = Ch$ and use the two blobs of the previous example. Figures 2-3 show the results.

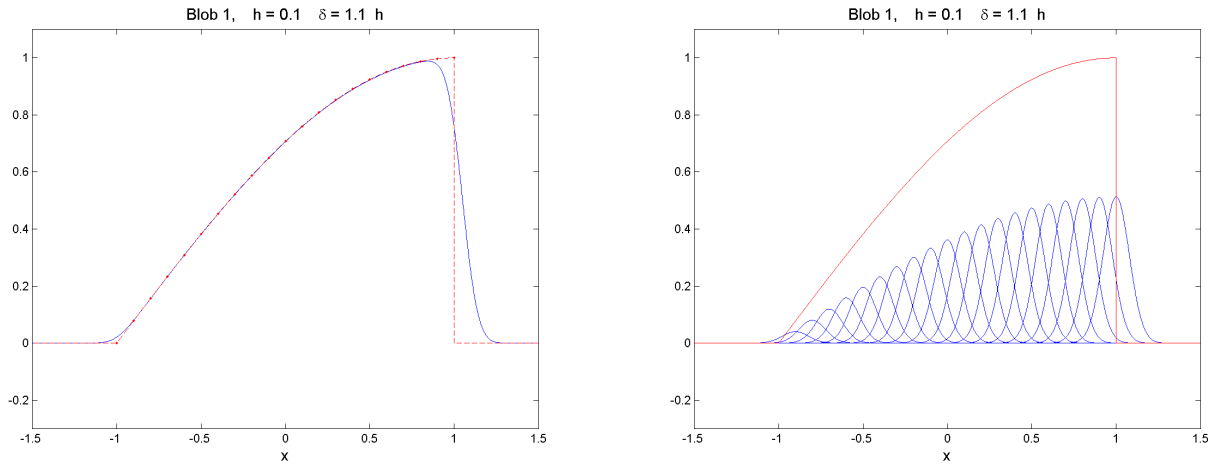

Figure 2: Blob approximation of the data in example 1.2 with ϕ_1.

The solid curve is the approximation given by the blob; the dots represent the given data. Notice that the approximation is very good away from the endpoints of the interval. Near the endpoints there is a larger error. Note that the data represent a function that is discontinuous at the right end of the interval (at $x = b$); this is because we assume

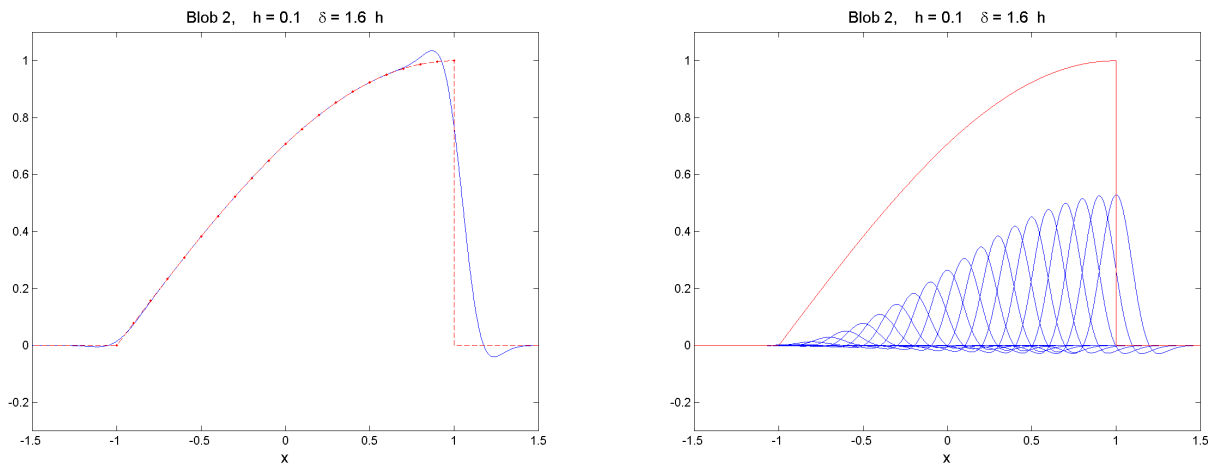

Figure 3: Blob approximation of the data in example 1.2 with ϕ_2.

that the function is zero outside the interval. But the blob approximation will always be continuous because it is a sum of smooth, continuous functions. So, it is not surprising that there is some difficulty approximating a discontinuous function. At the left endpoint ($x = a$), the function is continuous but the derivative is discontinuous (the function has a corner). This also causes the error to be somewhat larger there.

A natural question is then, how can δ be chosen relative to the particle spacing, so that the errors are as small as possible?

To attempt to answer this question, let's make a set of experiments. The function that we will try to approximate is $f(x) = \cos(\pi(x-1)/4)$ for $0 \le x \le 2$ and $f(x) = 0$ outside this interval. This is the same function of the previous example, which has a discontinuity at $x = 1$ and a corner at $x = -1$.

The results are shown in Figure 4-5.

The final experiment is one in which we set $\delta = Ch$ as we use more and more data points. This way, both h and δ are reduced together. The plots in Figure 6 show that the approximation gets better since h is decreasing and that the discontinuity is also better approximated because δ is also decreasing leading to less smearing.

Since the convolution approximates the function f with $O(\delta)$ (because f is discontinuous), then the trapezoid rule in Eq. (1) converges to the function f as $h, \delta \to 0$ together. For a smoother function f, the convergence would be faster.

MATLAB example

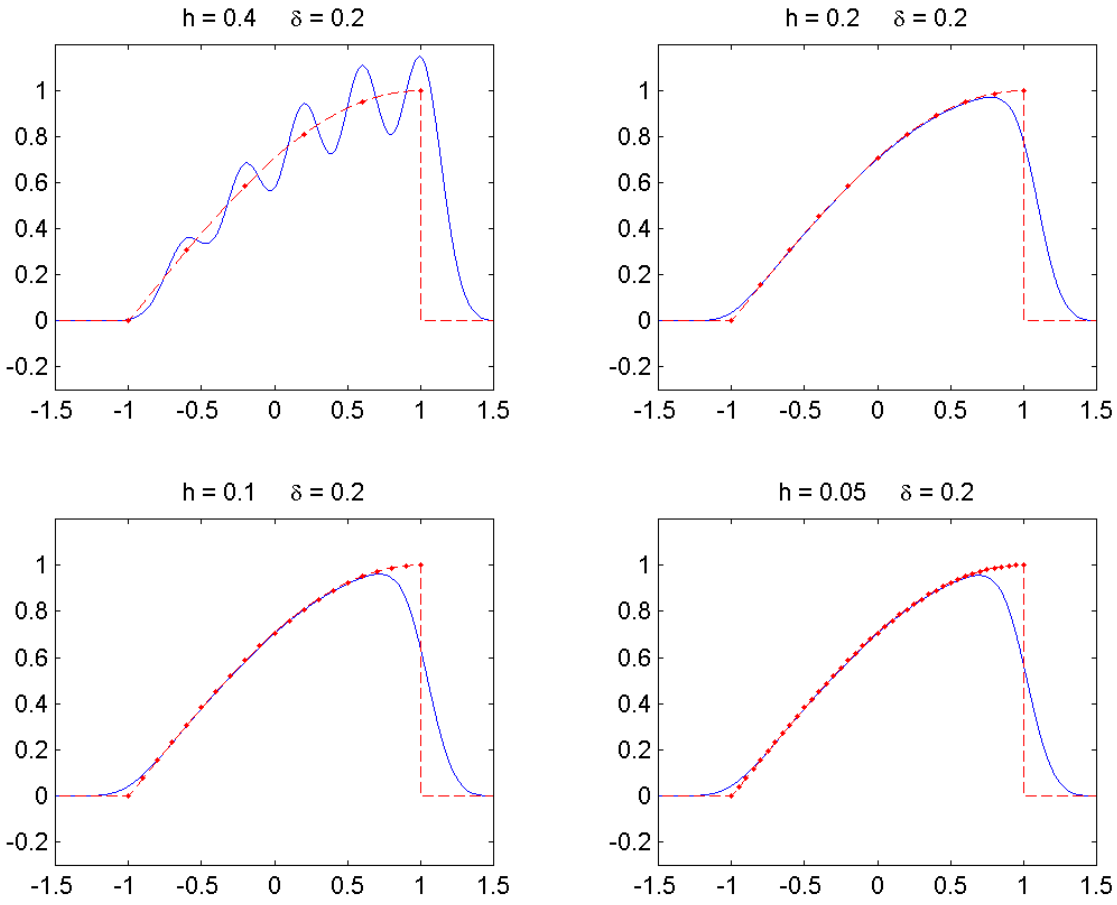

Figure 4: Blob approximations for various values of h and $\delta = 0.2$.

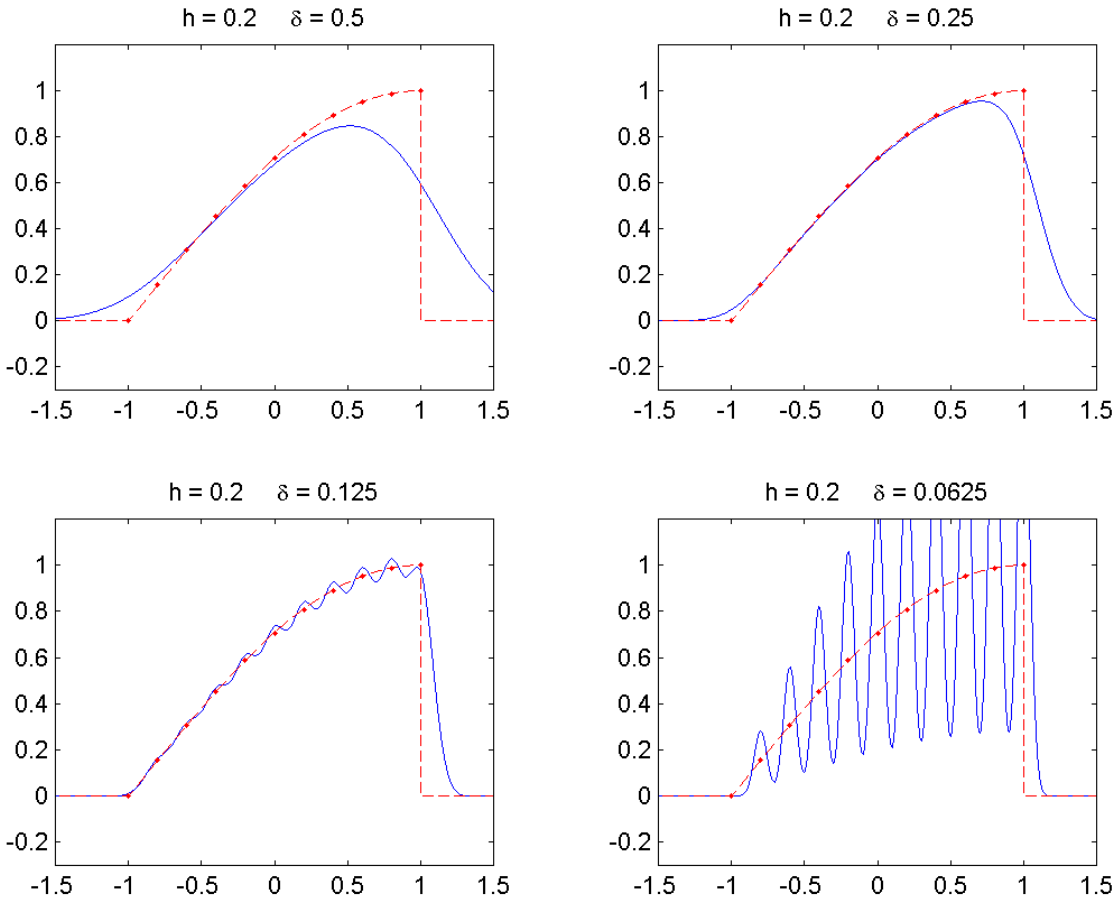

Figure 5: Blob approximations for $h = 0.2$ and various values of δ.

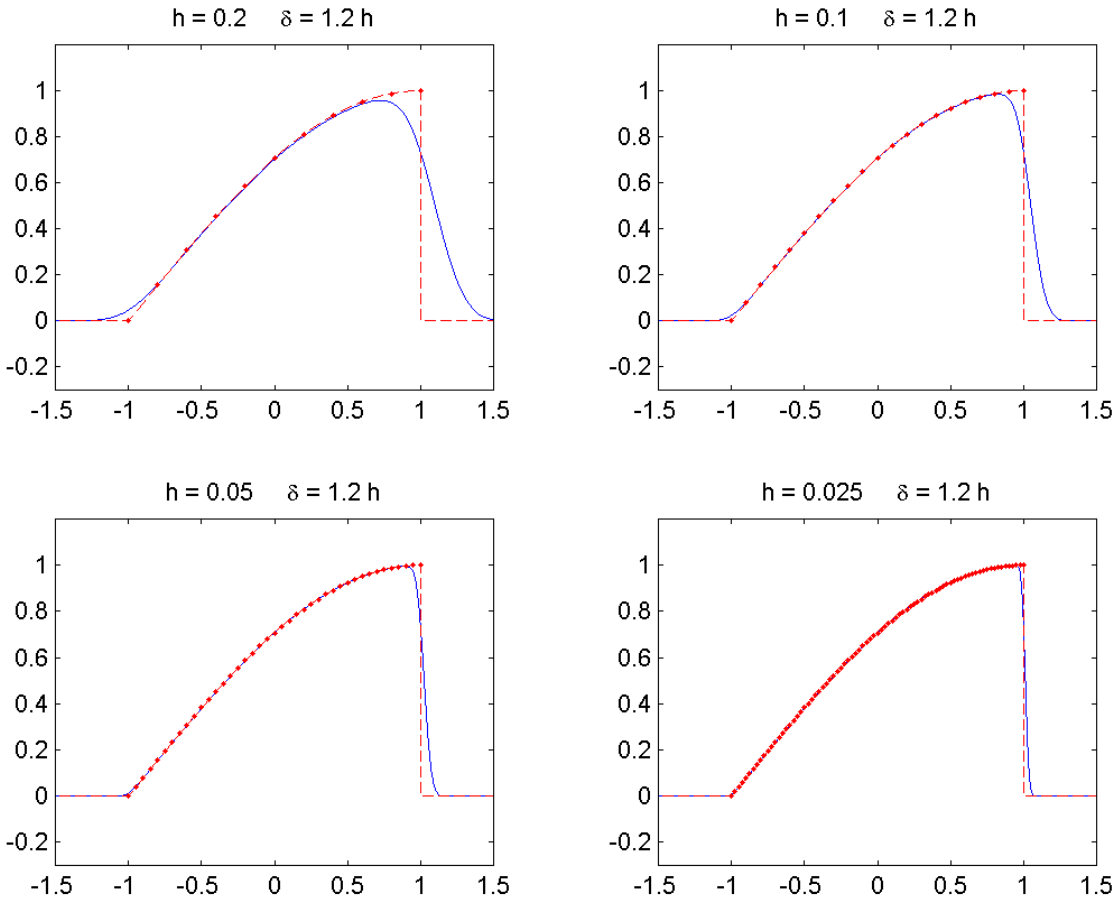

Figure 6: Blob approximations for various values of h and δ.

1.2 Blobs and regularized Green's functions in 1D

In 1D, Laplace's equation is simply $G''_\delta(x) = \phi_\delta(x)$. Suppose we choose the blob

$$\phi_\delta(x) = \frac{\delta^2}{2(x^2+\delta^2)^{3/2}} \tag{2}$$

then the general solution of $G''_\delta(x) = \phi_\delta(x)$ is

$$G_\delta(x) = \frac{1}{2}\sqrt{x^2+\delta^2} + \frac{1}{2}x + Ax + B.$$

For a function that is symmetric about the the y-axis, we choose $B = 0$ (arbitrary) and $A = -1/2$. This gives

$$G_\delta(x) = \frac{1}{2}\sqrt{x^2+\delta^2}. \tag{3}$$

Note that in the limit as δ vanishes we get the well-known result

$$\lim_{\delta\to 0} G_\delta(x) = \frac{1}{2}|x|.$$

In fact, the regularized Green's function in Eq. (3) satisfies for $\delta/|x| \ll 1$

$$G_\delta(x) = \frac{1}{2}|x| + O(\delta^2/x^2).$$

A second choice of blob

$$\phi_\delta(x) = \frac{3\delta^4}{4(x^2+\delta^2)^{5/2}} \tag{4}$$

yields the regularized Green's function

$$G_\delta(x) = \frac{1}{2}\sqrt{x^2+\delta^2} - \frac{\delta^2}{4\sqrt{x^2+\delta^2}}. \tag{5}$$

Note that this regularized Green's function also has the same limit as $\delta \to 0$. However, the function shown in Eq. (5) satisfies for $\delta/|x| \ll 1$

$$G_\delta(x) = \frac{1}{2}|x| + O(\delta^4/x^4).$$

The difference is easily seen in Figure 7. The dashed curve deviates from $|x|/2$ by a much smaller amount than the dash-dot curve. Notice that the second blob has a faster decay rate at infinity.

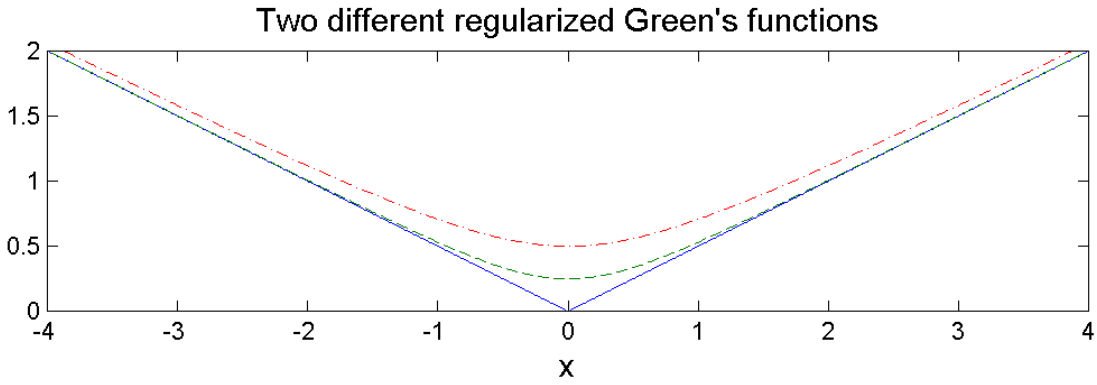

Figure 7: Green's functions in Eq. (3) and Eq. (5) for $\delta = 1$.

It is also possible to derive Green's functions from blobs with compact support and even discontinuous blobs. As an example, consider the *step* blob

$$\phi_\delta(x) = \begin{cases} \frac{1}{2\delta}, & |x| < \delta \\ 0, & |x| \geq \delta. \end{cases} \tag{6}$$

Since we are required to solve $G''_\delta(x) = \phi_\delta(x)$, after integrating once, we find

$$G'_\delta(x) = \begin{cases} (A - 1/2), & x < -\delta \\ \frac{x}{2\delta} + A, & |x| \leq \delta \\ (A + 1/2), & x > \delta \end{cases}$$

and after integrating once more, we have

$$G_\delta(x) = \begin{cases} (A - 1/2)x + (B - \delta/4), & x < -\delta \\ \frac{x^2}{4\delta} + Ax + B, & |x| \leq \delta \\ (A + 1/2)x + (B - \delta/4), & x > \delta. \end{cases}$$

In order to match the Green's function $|x|/2$ for $|x| > \delta$, we can choose $A = 0$ and $B = \delta/4$, so that

$$G_\delta(x) = \begin{cases} |x|/2, & |x| \geq \delta \\ \frac{\delta}{4}\left(\frac{x^2}{\delta^2} + 1\right), & |x| < \delta \end{cases}$$

which is a $C^1(\mathbb{R})$ function. We emphasize that this regularized Green's function differs from $|x|/2$ only in the support of the blob.

2 Blobs in two dimensions

In two dimensions we require that a blob $\phi(x, y)$ have total integral $\int_{\mathbb{R}^2} \phi = 1$. One possibility is to define radially symmetric blobs $\phi(r)$ so that $2\pi \int_0^\infty r\phi(r)dr = 1$. Examples of these functions are

$$\phi(r) = \frac{1}{\pi}\, e^{-r^2} \quad \textit{and} \quad \phi(r) = \frac{3}{2\pi(r^2+1)^{5/2}}.$$

In two dimensions a blob ϕ_δ is scaled by area:

$$\phi_\delta(x) = \frac{1}{\delta^2}\phi(x/\delta)$$

where the scaling parameter δ is small.

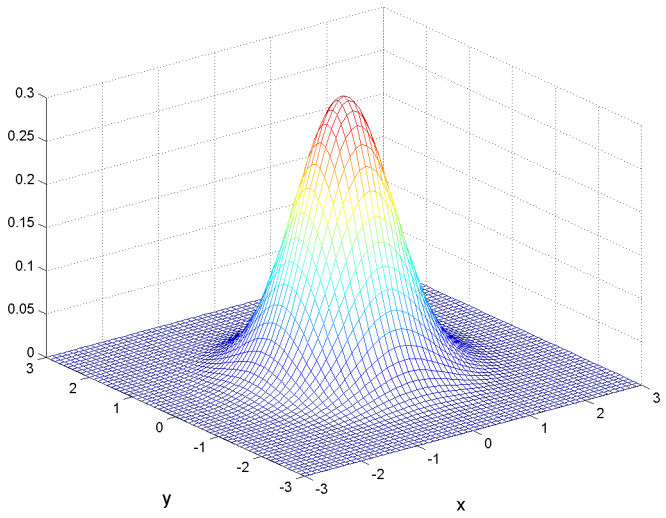

Figure 8: Sample blob in two dimensions.

In this case, the convolution of a function $f(\vec{x})$ with a blob is

$$(f \star \phi_\delta)(\vec{x}) = \int_{-\infty}^{\infty} \int_{-\infty}^{\infty} f(\vec{y}) \phi_\delta(\vec{x} - \vec{y}) d\vec{y}$$

The moments for radially symmetric blobs are

$$M_k(\phi) = C(k) \int_0^\infty r^{k+1} \ \phi(r) \ dr$$

and if we design a blob with $M_0 = 1$ and $M_k = 0$ for $k = 1, \ldots, p-1$ then $(f \star \phi_\delta) - f = O(\delta^p)$.

NOTE: The odd moments are automatically zero due to symmetry.

The numerical approximation of this double integral is done in a similar way as in the one-dimensional case. Suppose first that the function $f : \mathbb{R}^2 \to \mathbb{R}$ is zero outside some bounded set $\Omega \in \mathbb{R}^2$. We then subdivide the set Ω into small areas A_k for $k = 1, 2, \cdots, N$ (for example, $A_k = h^2$ if we use a grid) and we let $\vec{y}_k$ denote the *center* of area A_k. Then we can write

$$(f \star \phi_\delta)(\vec{x}) \approx \sum_{k=1}^{N} f(\vec{y}_k) \phi_\delta(\vec{x} - \vec{y}_k) A_k$$

2.1 Regularized Green's functions in two dimensions

In general, given the blob $\phi_\delta(r)$, we must solve $\Delta G_\delta = \phi_\delta$. In polar coordinates we write

$$\Delta G_\delta = \frac{\partial^2 G_\delta}{\partial r^2} + \frac{1}{r}\frac{\partial G_\delta}{\partial r} + \frac{1}{r^2}\frac{\partial^2 G_\delta}{\partial \theta^2}.$$

We assume that the *diffusion* of any quantity is symmetric with respect to r, that is, G_δ does not depend on θ. Then we only need to solve the ODE

$$G_\delta''(r) + \frac{1}{r}G_\delta'(r) = \frac{1}{r}\left[rG_\delta'(r)\right]' = \phi_\delta(r)$$

For example, suppose the blob is given by

$$\phi_\delta(r) = \frac{\delta^2}{\pi(r^2+\delta^2)^2} \tag{7}$$

and we integrate the above equation once to get

$$rG_\delta'(r) = \frac{r^2}{2\pi(r^2+\delta^2)}$$

and integrating once more, we get

$$G_\delta(r) = G_\delta(0) + \frac{1}{2\pi}\ln(\sqrt{r^2+\delta^2}) - \frac{1}{2\pi}\ln(\delta).$$

The constant $G_\delta(0)$ is arbitrary. Here we choose it to eliminate the last term so that

$$G_\delta(r) = \frac{1}{2\pi}\ln(\sqrt{r^2+\delta^2}). \tag{8}$$

Notice that

$$\lim_{\delta\to 0} G_\delta(r) = \frac{1}{2\pi}\ln(r)$$

which is the well-known Green's function for the Laplacian in two dimensions. The function G_δ is called a *regularized Green's function*, and it depends on the blob used to derive it. For example, we might use instead of Eq. (7) the blob

$$\phi_\delta(r) = \frac{\delta}{2\pi(r^2+\delta^2)^{3/2}} \tag{9}$$

and this leads to another regularized Green's function

$$G_\delta(r) = \frac{1}{2\pi}\ln(\sqrt{r^2+\delta^2}+\delta). \tag{10}$$

Although the specific form of the regularized Green's function depends on the choice of blob, they all share the properties that

$$\begin{aligned} \lim_{\delta \to 0} G_\delta(r) &= \frac{1}{2\pi} \ln(r) \quad \text{and} \\ \lim_{r \to \infty} |G_\delta(r) - \frac{1}{2\pi} \ln(r)| &= 0 \quad \text{for fixed } \delta. \end{aligned}$$

One can check that the regularized Green's function in Eq. (8) satisfies $G_\delta(r) = 1/2\pi \ln(r) + O(\delta^2/r^2)$ for $\delta/r \ll 1$ while the function in Eq. (10) satisfies $G_\delta(r) = 1/2\pi \ln(r) + O(\delta/r)$ for $\delta/r \ll 1$. This shows that different blobs of the same order can yield regularized Green's functions that approximate $\frac{1}{2\pi} \ln(r)$ to different orders of accuracy in δ for large values of r. This property seems to come from the decay rate of the blob as $r \to \infty$.

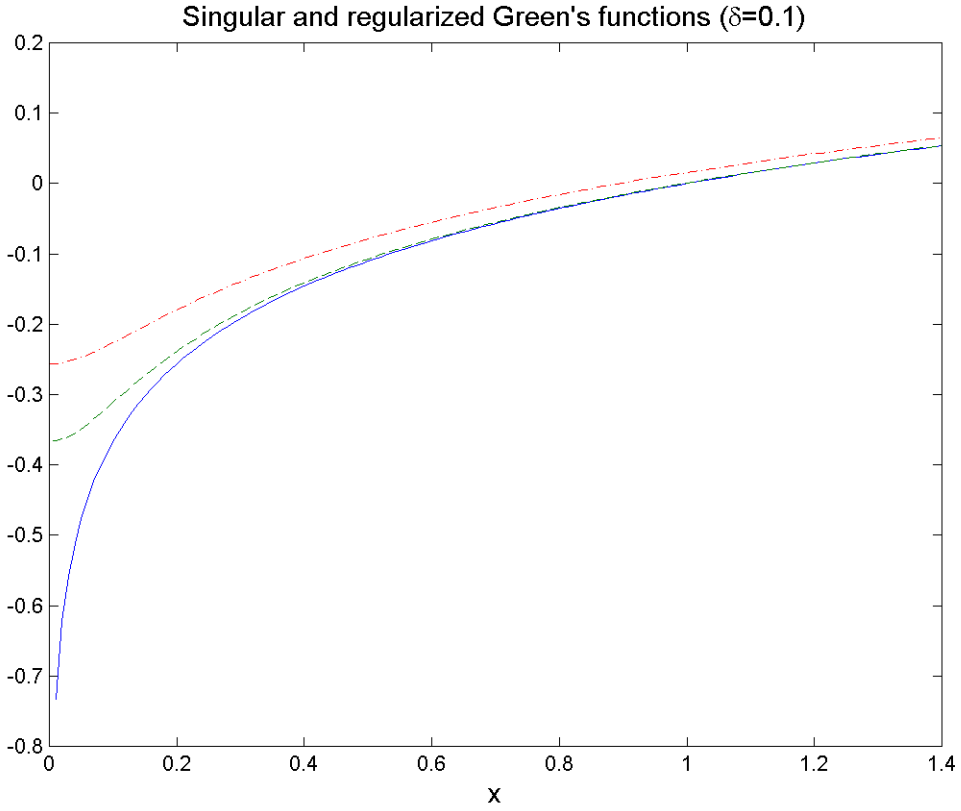

Figure 9: Singular and regularized Green's functions.

2.2 Application to vortex methods in 2D

In 2D incompressible flow, the fluid velocity (u, v) and the vorticity are related by $\nabla \cdot \mathbf{u} = 0$ and $\nabla \times \mathbf{u} =$vorticity.

Let a function $\psi(x, y, t)$ be such that

$$u = \psi_y \quad \text{and} \quad v = -\psi_x.$$

With this assumption, we can then determine the relationship between vorticity and ψ. We have that

$$\omega = v_x - u_y = -\psi_{xx} - \psi_{yy} = -\Delta\psi.$$

So, given the vorticity, we can solve for ψ and then obtain the velocity created by the vorticity by differentiating ψ. The vorticity is advected by the fluid flow.

Example 2.1 Consider the vorticity given by a single point vortex at $\mathbf{x}_0$:

$$\omega(x) = \omega_0 \delta(\mathbf{x} - \mathbf{x}_0).$$

Then

$$\Delta\psi = -\omega_0 \delta(\mathbf{x} - \mathbf{x}_0), \qquad \Rightarrow \qquad \psi = -\omega_0 G(\mathbf{x} - \mathbf{x}_0) = -\frac{\omega}{2\pi} \ln(r)$$

and the flow is $u = -\omega G_y = -\omega \frac{y - y_0}{2\pi r^2}$, $v = \omega G_x = \omega \frac{x - x_0}{2\pi r^2}$.

The singularity can be removed if we assume the vorticity is given by a blob

$$\omega(x) = \omega_0 \phi_\delta(\mathbf{x} - \mathbf{x}_0).$$

Then

$$\Delta\psi = -\omega_0 \phi_\delta(\mathbf{x} - \mathbf{x}_0), \qquad \Rightarrow \qquad \psi = -\omega_0 G_\delta(\mathbf{x} - \mathbf{x}_0)$$

and the flow is $u = -\omega \partial G_\delta / \partial y = -\omega G'_\delta(r) \frac{y - y_0}{r}$, $v = \omega \partial G_\delta / \partial x = \omega G'_\delta(r) \frac{x - x_0}{r}$.

As an example, the blob

$$\phi_\delta(r) = \frac{\delta^2}{\pi (r^2 + \delta^2)^2}$$

yields a regularized Green's function

$$G_\delta(r) = \frac{1}{2\pi} \ln(\sqrt{r^2 + \delta^2})$$

and therefore the particles move by

$$\begin{aligned} X'(T) &= -\omega \frac{Y}{X^2 + Y^2 + \delta^2}, \qquad X(0) = x_o \\ Y'(T) &= \omega \frac{X}{X^2 + Y^2 + \delta^2}, \qquad Y(0) = y_o. \end{aligned}$$

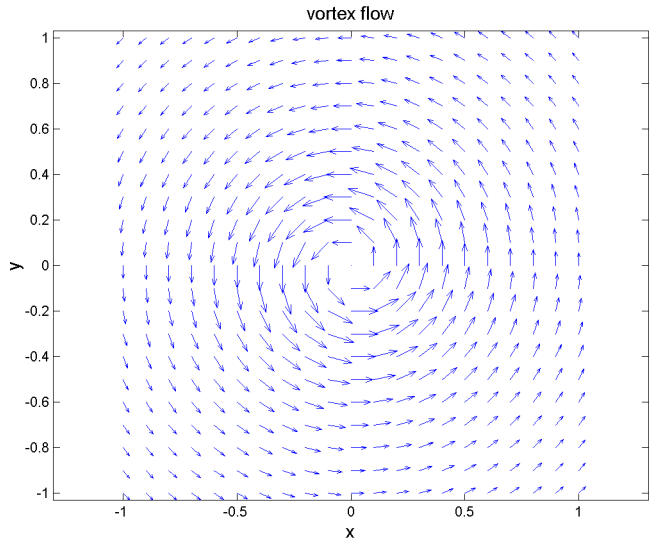

Figure 10: Vortex flow.

3 Blobs in three dimensions

In three dimensions we require that a blob $\phi(x, y, z)$ have total integral $\int_{\mathbb{R}^3} \phi = 1$. One possibility is to define radially symmetric blobs $\phi(r)$ so that $4\pi \int_0^\infty r^2 \phi(r) dr = 1$. Examples of these functions are

$$\phi(r) = \frac{15}{8\pi(r^2+1)^{7/2}}. \quad \textit{and} \quad \phi(r) = \frac{3}{4\pi(r^2+1)^{5/2}}.$$

In three dimensions a blob ϕ_δ is scaled by volume:

$$\phi_\delta(x) = \frac{1}{\delta^3}\phi(x/\delta)$$

where the scaling parameter δ is small.

The moments for radially symmetric blobs are

$$M_k(\phi) = C(k) \int_0^\infty r^{k+2}\ \phi(r)\ dr$$

and if we design a blob with $M_0 = 1$ and $M_k = 0$ for $k = 1, \ldots, p-1$ then $(f \star \phi_\delta) - f = O(\delta^p)$.

NOTE: Several moments are automatically zero due to symmetry.

3.1 Regularized Green's functions in three dimensions

In three dimensions, the Laplacian operator in spherical coordinates is

$$\Delta f(r,\theta,\varphi) = f_{rr} + \frac{2}{r} f_r + \frac{1}{r^2 \sin\theta} (\sin\theta f_\theta)_\theta + \frac{1}{r^2 \sin^2\theta} f_{\varphi\varphi}.$$

But one can argue that since $\phi_\delta(r)$ is independent of θ and φ and since $\Delta G_\delta = \phi_\delta$, then the Green's function must also be independent of θ and φ. So we consider the equation

$$G_\delta''(r) + \frac{2}{r} G_\delta'(r) = \frac{1}{r^2}[r^2 G_\delta'(r)]' = \phi_\delta(r).$$

We can proceed in the same way we did in two dimensions. For the blob

$$\phi_\delta(r) = \frac{3}{4\pi(r^2+\delta^2)^{5/2}} \tag{11}$$

we find that

$$r^2 G_\delta'(r) = \int_0^r s^2 \phi_\delta(s) ds = \frac{r^3}{4\pi(r^2+\delta^2)^{3/2}}$$

so that

$$G_\delta(r) = G_\delta(0) + \frac{1}{4\pi\delta} - \frac{1}{4\pi\sqrt{r^2+\delta^2}}.$$

If we choose $G_\delta(0) = -1/4\pi\delta$ to eliminate the constant term, we have that

$$G_\delta(r) = \frac{-1}{4\pi\sqrt{r^2+\delta^2}}. \tag{12}$$

Note that

$$\lim_{\delta\to 0} G_\delta(r) = \frac{-1}{4\pi r}$$

which is the familiar Green's function for the Laplacian in three dimensions. In this case, one can see that

$$G_\delta(r) = \frac{-1}{4\pi r} + O(\delta^2/r^2) \quad \text{for } \delta/r \ll 1$$

3.2 Application to Stokes flows in 3D

The Stokes equations for incompressible flow without boundaries are

$$\mu\Delta\mathbf{u} - \nabla p = -\mathbf{F}, \qquad \nabla\cdot\mathbf{u} = 0$$

Suppose the external force is given by $\mathbf{F}(\mathbf{x}) = \mathbf{f}_0\phi_\delta(\mathbf{x}-\mathbf{x}_0)$.

Define once and for all the functions G_δ and B_δ by

$$\Delta G_\delta = \phi_\delta, \qquad \Delta B_\delta = G_\delta$$

Take divergence of the first equation and get

$$\Delta p = \mathbf{f}_0 \cdot \nabla \phi_\delta \qquad \Rightarrow \qquad p = \mathbf{f}_0 \cdot \nabla G_\delta$$

Now,

$$\mu \Delta \mathbf{u} = (\mathbf{f}_0 \cdot \nabla) \nabla G_\delta - \mathbf{f}_0 \phi_\delta$$

Yielding

$$\mu \mathbf{u} = (\mathbf{f}_0 \cdot \nabla) \nabla B_\delta - \mathbf{f}_0 G_\delta$$

This is called a Regularized Stokeslet. In general, the strategy to compute Stokes flows is:

- choose a blob ϕ_δ and find G_δ and B_δ
- given forces $\mathbf{f}_k$ located at $\mathbf{x}_k$, compute

$$\mu \mathbf{u}(\mathbf{x}) = \sum_k (\mathbf{f}_k \cdot \nabla) \nabla B_\delta(\mathbf{x} - \mathbf{x}_k) - \mathbf{f}_k G_\delta(\mathbf{x} - \mathbf{x}_k)$$

  to show the velocity at any point $\mathbf{x}$ or compute $d\mathbf{x}_j/dt = \mathbf{u}(\mathbf{x}_j)$ to update particle positions.

Example 3.1 Consider a body falling under it own weight in a Stokes flow. Every point on the surface of the body exerts an equal force on the fluid. Thus, the velocity at any point in the fluid is given by the regularized Stokeslet formula (see figures 11 and 12).

3.3 More about fluid flows

So far, we have an expression for the velocity of a Stokes flow generated by forces $\mathbf{f}_k$ applied at positions $\mathbf{x}_k$. *What if we apply a torque instead of a force? What if we apply pairs of forces?*

There are other known solutions to the Stokes equations that are typically generated by taking derivatives of the Stokeslet solution. For example, given the (singular) Stokeslet expression:

$$S(\mathbf{x} - \mathbf{x}_0) = (\mathbf{f}_0 \cdot \nabla) \nabla B(\mathbf{x} - \mathbf{x}_0) - \mathbf{f}_0 G(\mathbf{x} - \mathbf{x}_0)$$

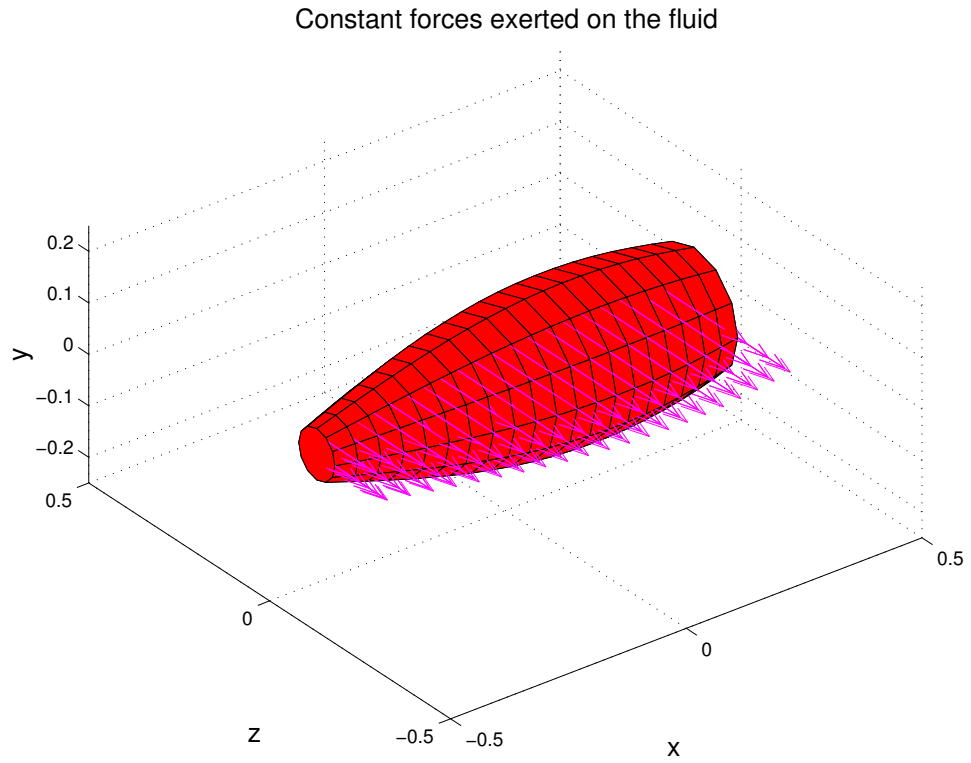

Figure 11: Forces on a body falling in Stokes flow.

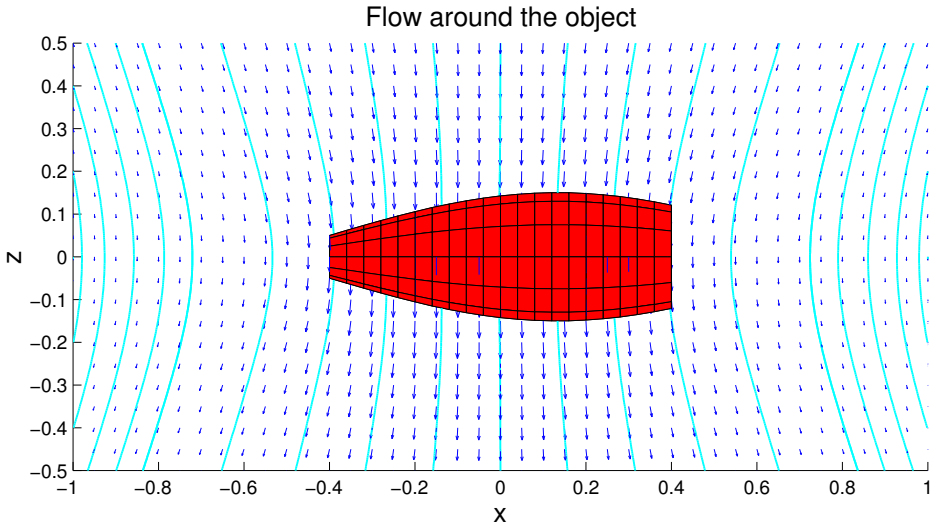

Figure 12: Velocity around a body falling in Stokes flow.

A *Doublet* is defined as

$$Doub_i(\mathbf{x}-\mathbf{x}_0) = -\frac{\partial}{\partial \mathbf{x}_i} S(\mathbf{x}-\mathbf{x}_0).$$

A *Dipole*, given by

$$Dip(\mathbf{x}-\mathbf{x}_0) = -\Delta S(\mathbf{x}-\mathbf{x}_0)$$

represents the flow due to a pair of equal and opposite vortices near each other.

A *Rotlet* of strength $\mathbf{L}$ applied at $\mathbf{x}_0$ is given by

$$R(\mathbf{x}-\mathbf{x}_0) = \mathbf{L} \times \nabla G(\mathbf{x}-\mathbf{x}_0)$$

and represents the flow due to a torque $\mathbf{L}$. There are others. Regularized versions of all of these elements can be derived based on blobs.

What if the flow is not Stokes?

In other types of flows, like Euler flows, there are solutions like the vortex blob method that are known in regularized form. Dipoles are also solutions of Euler flows.

4 Applications

4.1 Motion of a 2D swimming sheet in a viscous flow

We consider a "curve" in 2D where there is a defined force field. The curve may represent a swimming organism. The time-dependent forces exerted on the fluid by the organism generate the flow which interacts with the motion of the organism.

Go to eel site

4.2 Flow in a 2D channel with point obstacles

Consider a channel in two dimensions with a background flow $\mathbf{U} = (1, 0)$ (or parabolic). Now imagine there are point obstacles which cannot move, therefore the flow must go around them. This flow can be computed by allowing each obstacle and each boundary point to exert a force on the fluid with the purpose of satisfying the conditions that the velocity must equal zero at all the points shown in Figure 14.

In order to compute this flow, we note that in the regularized Stokeslet formula

$$\mathbf{u}(\mathbf{x}) = \sum_{k=1}^{N} (\mathbf{f}_k \cdot \nabla)\nabla B(\mathbf{x}-\mathbf{x}_k) - \mathbf{f}_k G(\mathbf{x}-\mathbf{x}_k)$$

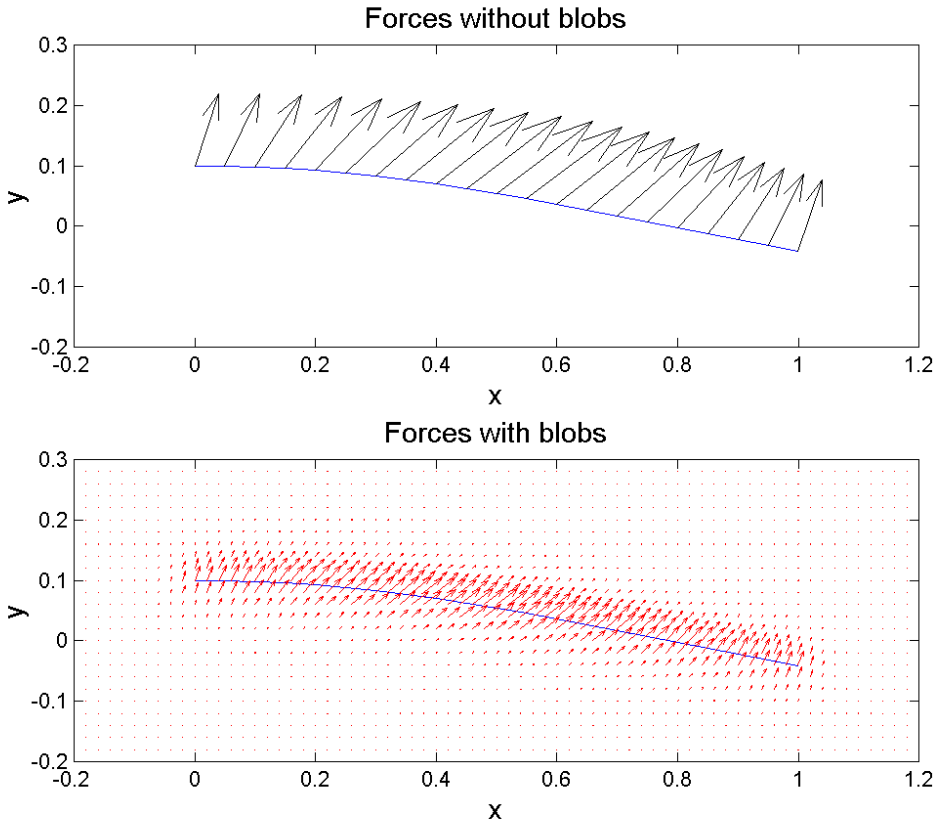

Figure 13: Forces along a curve are spread over the surrounding region.

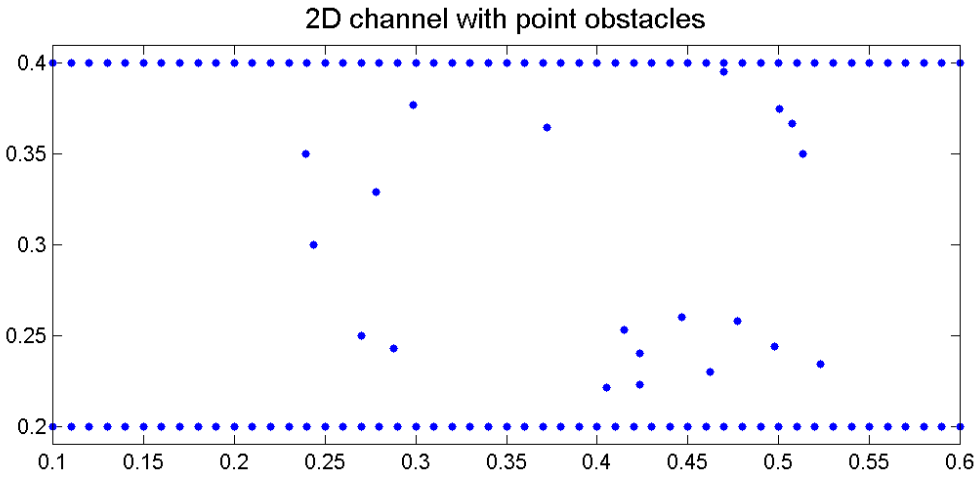

Figure 14: Channel with point obstacles.

the velocity at any point $\mathbf{x}$ depends linearly on the forces $\mathbf{f}_k$. Therefore, if the velocity at each of the points $\mathbf{x}_k$ must equal zero, we can set up the system of equations

$$\mathbf{u}(\mathbf{x}_j) = -\mathbf{U} = \sum_{k=1}^{N} (\mathbf{f}_k \cdot \nabla)\nabla B_\delta(\mathbf{x}_j - \mathbf{x}_k) - \mathbf{f}_k G_\delta(\mathbf{x}_j - \mathbf{x}_k)$$

for $j = 1, 2, \ldots, N$. This is a linear system of $3N$ equations for the $3N$ components of the forces. If the matrix is nonsingular, there is a unique solution for the forces. Once the forces have been found, the velocity at points inside the channel can be computed by superimposing the regularized Stokeslet formula and the background flow to display the flow as in Figure 15.

$$\mathbf{u}(\mathbf{x}) = \mathbf{U} + \sum_{k=1}^{N} (\mathbf{f}_k \cdot \nabla)\nabla B(\mathbf{x} - \mathbf{x}_k) - \mathbf{f}_k G(\mathbf{x} - \mathbf{x}_k)$$

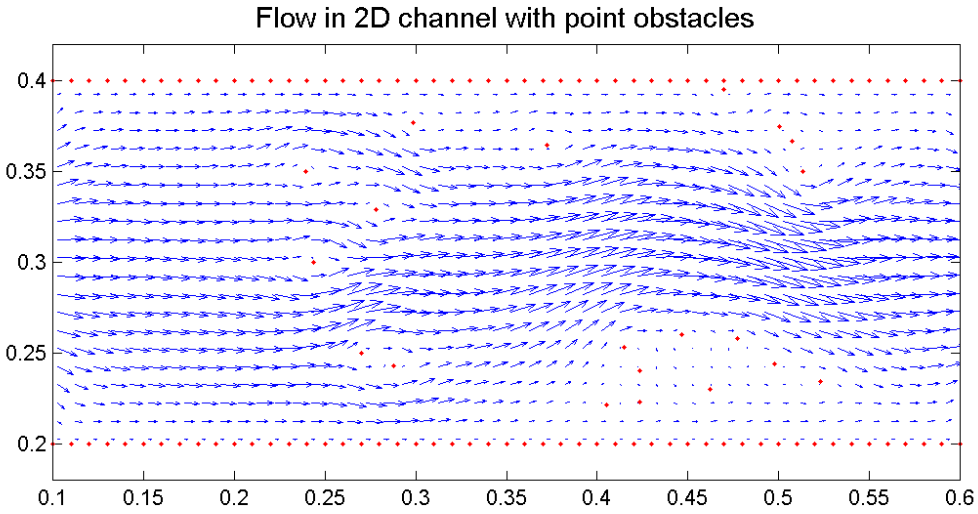

Figure 15: Velocity field in the channel with point obstacles.

Go to matlab

4.3 Motion of a 3D helical swimmer in Stokes flow

A helical swimmer here means an elastic tube in the shape of a helix that is rotated by an external torque (or by external forces) and as it rotates, its shape forces it to translate like a corkscrew.

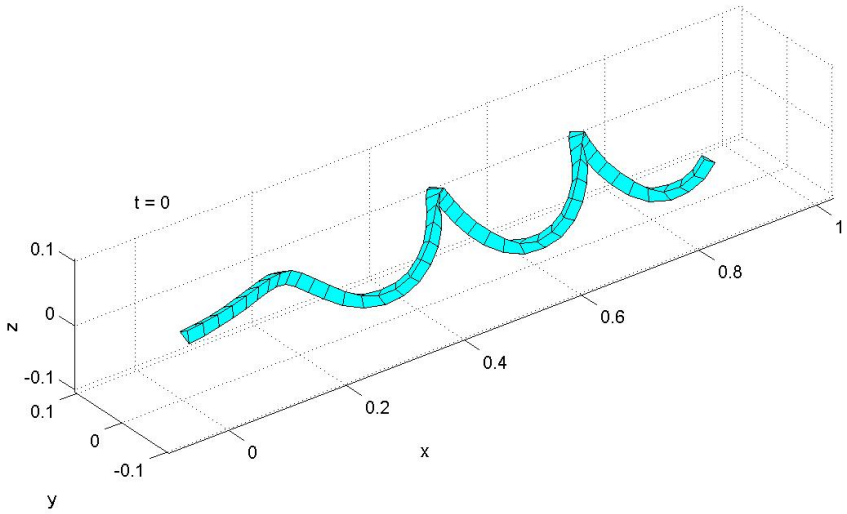

Figure 16: Constructed helical swimmer.

In the following model, the tube is made of a series of rings that are centered and perpendicular to a helical centerline. The points on the rings are connected by springs and additional springs connect points on one ring to points on neighboring rings. The motion is generated by either a torque at the nose of the organism or forces that make it rotate. The rotation causes the springs to stretch and contract generating forces along the entire organism. Each force contributes to the flow through a regularized Stokeslet and the torque through a rotlet.

Go to animation of single helix.

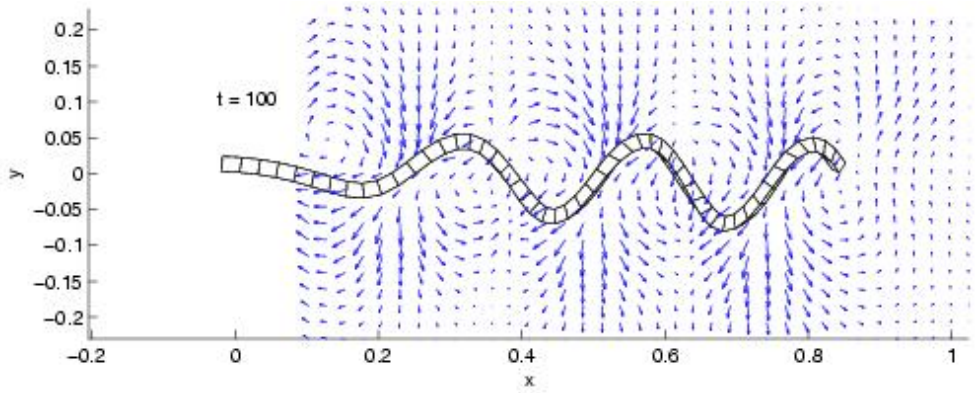

Figure 17: Instantaneous velocity field around the helical swimmer.

4.4 Flagellar bundling in a 3D Stokes flow

Some bacteria such as *E. coli* and *Salmonella* have a large cell body and many flagella that are used to propel the cell as it consumes nutrient.

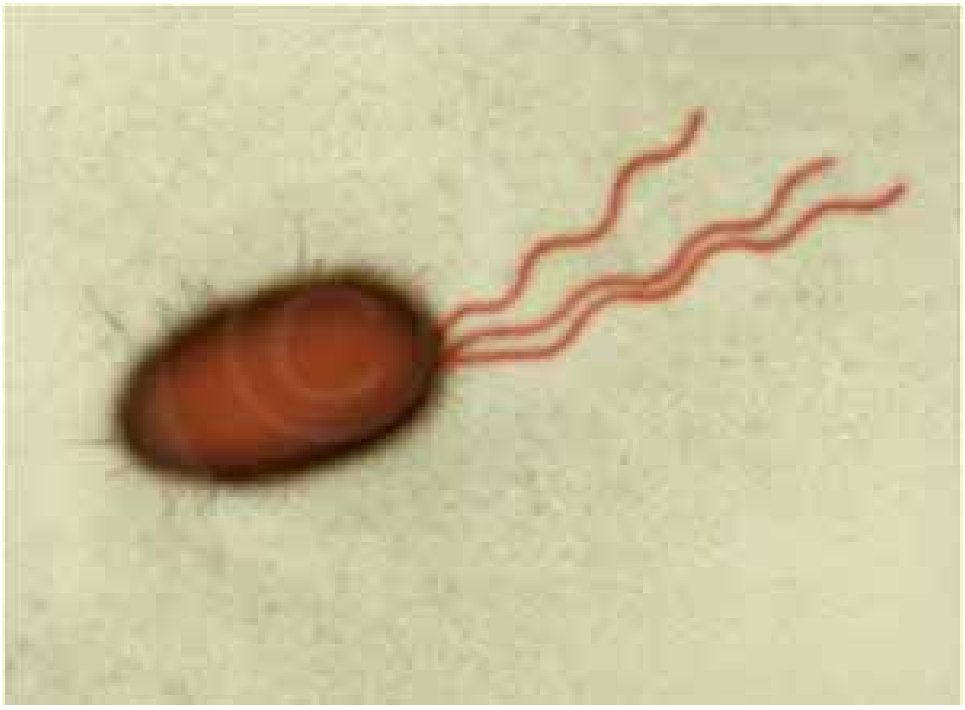

Figure 18: E. coli photo taken from http://www.le.ac.uk/biology/research/phyto/antibody.htm

At the point where each flagellum is attached to the cell body there is a motor that rotates the flagellum in either direction. When all motors rotate in one direction, the flagella tend to bundle into a single tail that helps propel the bacteria. When one or

more motors rotate in the opposite direction, the flagella tend to come apart and the cell moves erratically until the motors synchronize again and the flagella bundle, moving the cell in a new direction.

A model of three flagella (without a body) was constructed in the same way as before and each motor at the front of the flagella was modeled by a torque.

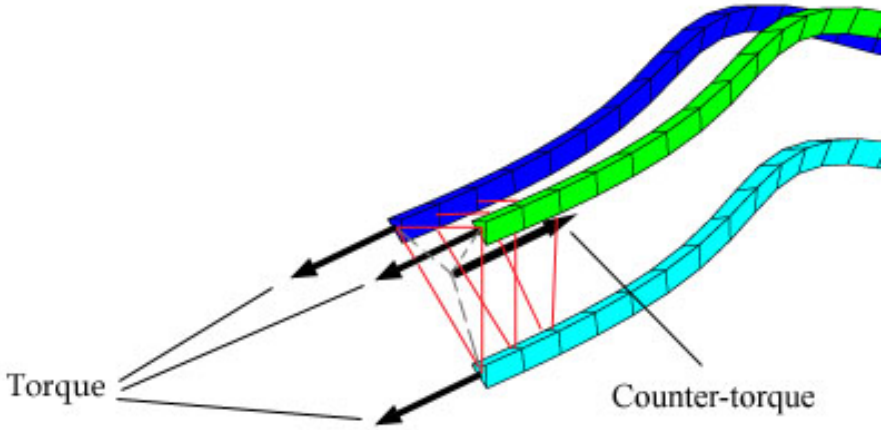

Figure 19: Schematic of the three-flagellum configuration.

Go to animation of bundling and tumbling

4.5 Flow due to moving objects near a wall (method of images)

So far, the solutions have been based on the free-space Green's function. In the case of the channel flow, the channel walls were discretized in order to satisfy the appropriate boundary conditions. The walls must be of finite extent since we cannot tile an infinite wall with points.

When there is an object moving close to an infinite wall, one approach to satisfying boundary conditions at the wall is to use the method of images. In this method, one places forces, dipoles, vortices or other elements at the mirror image points on the other side of the wall and adjusts their strengths to satisfy the appropriate boundary conditions.

For example, a vortex in 2D Euler flow (zero viscosity) near a wall at $y = 0$ must satisfy the conditions that the velocity at the wall must not contain a component normal to the flow. The tangential component (slip velocity) may exist in the absence of viscosity. In order to cancel the normal velocity at the wall due to one vortex, one may place an equal

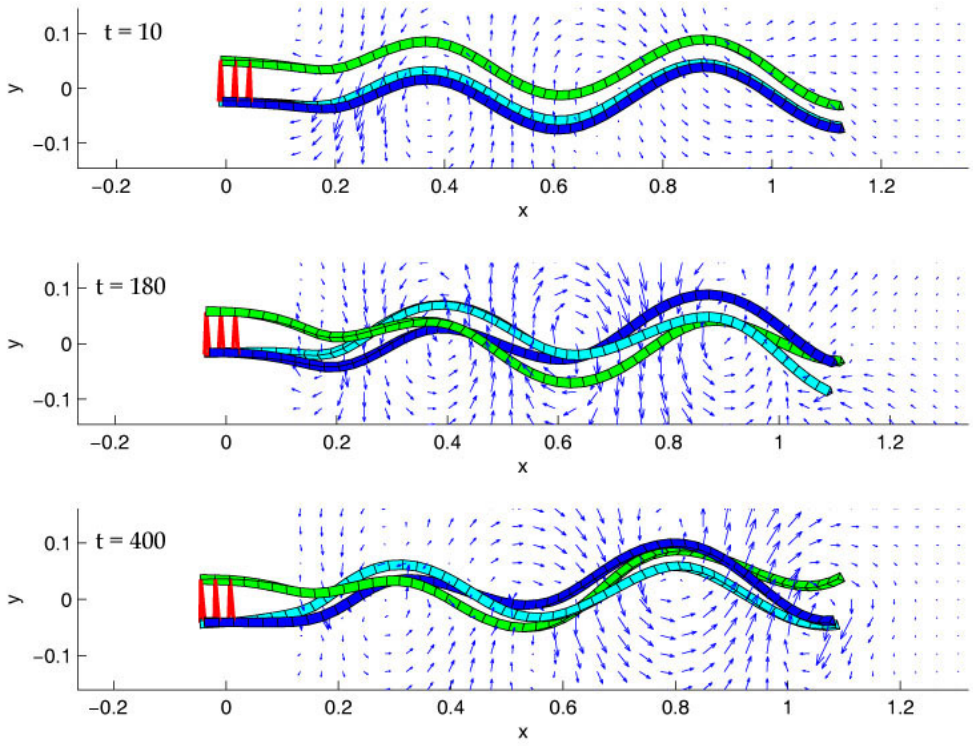

Figure 20: Flow around the three flagella.

and opposite vortex at the image point.

Something similar can be done in Stokes flows due to forces. At the image point, one must place a regularized Stokeslet, doublet, dipole and rotlet in order to satisfy the zero-velocity boundary condition.

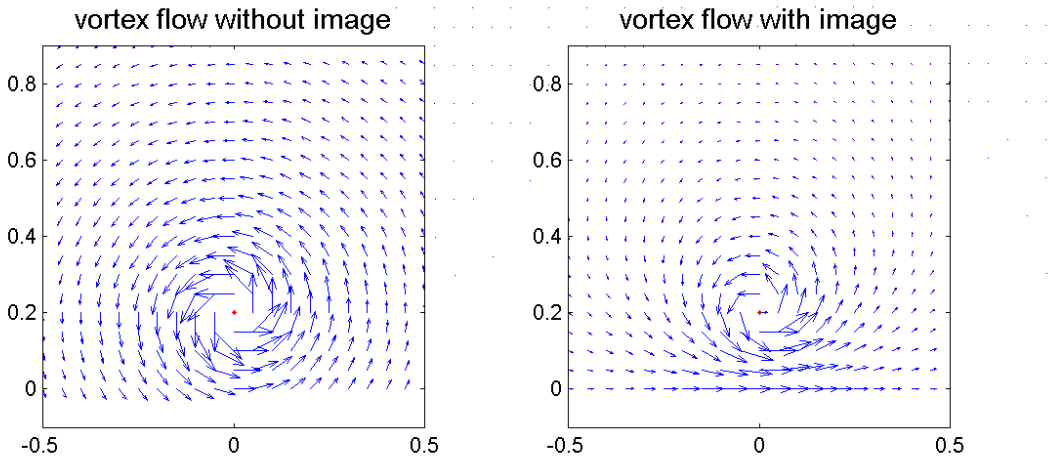

Figure 21: Flow due to a single vortex in free space (left) and next to an infinite wall (right).

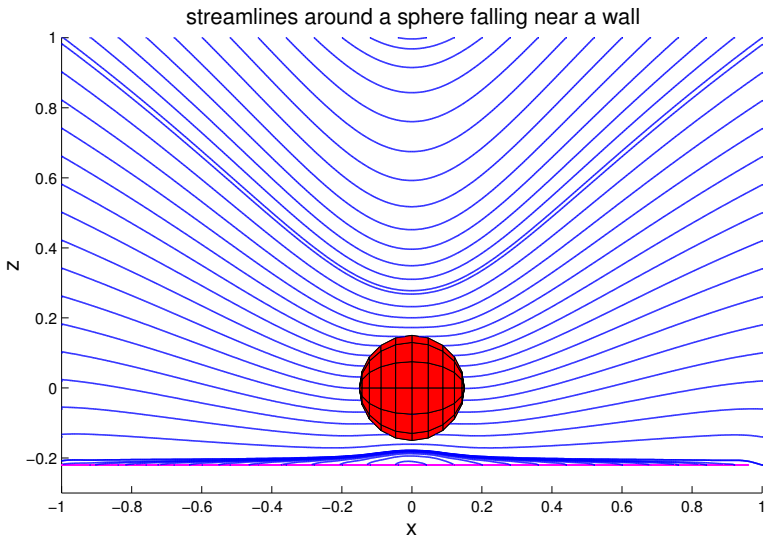

Figure 22: Ball falling near a wall.

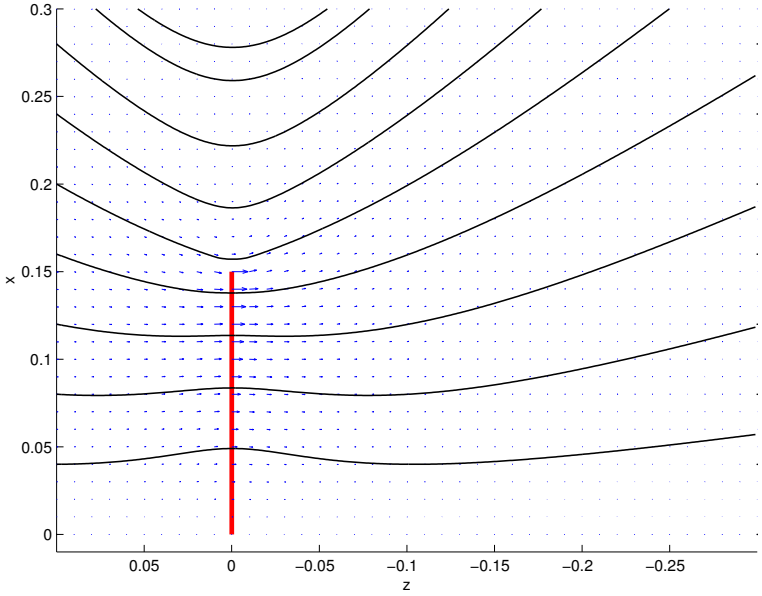

Figure 23: Power stroke of a cilium.

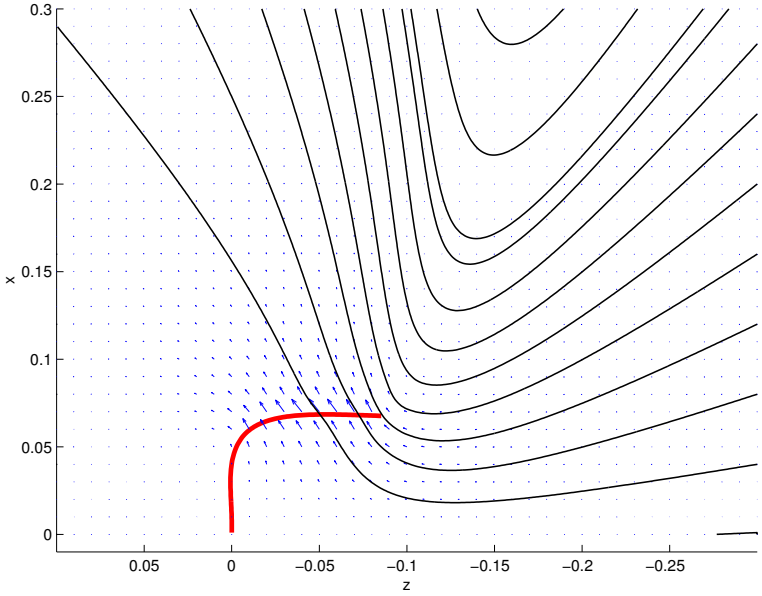

Figure 24: Recovery stroke of a cilium.